

# A circular microchannel with integrated electrodes for DNA electrophoresis

B. Lerner · P. A. Kler · A. F. Ordoñez Arias ·  
M. S. Perez · C. Lasorsa · C. L. A. Berli

Received: 13 August 2012 / Accepted: 24 September 2012  
© Springer-Verlag Berlin Heidelberg 2012

**Abstract** The development of a novel microfluidic device that includes a circular microchannel and integrated electrodes for DNA electrophoresis is reported. The geometry of the separation channel and the arrangement of the embedded electrodes provide several advantages in relation to conventional linear microchannels. The paper describe the design, modeling, construction, and testing of the micro device. Numerical simulations were used to investigate the electric field into the microchannel. In addition, the electrophoretic transport of DNA samples was studied under different voltage configurations. The experiments reported show the functionality of the device, and illustrate interesting features of DNA transport.

## 1 Introduction

Electrophoresis is a widely used method in biology and biotechnology labs for the separation and analysis of DNA and proteins (Andrews and Andrews 1986; Hames 1998). In the last two decades, electrophoretic techniques have substantially evolved, driven by the ambitious programs of genetic engineering (genomics and proteomics). In particular, the implementation of capillary electrophoresis on silicon chips (Harrison et al. 1993) led to a considerable gain of time and performance, while the volumes of sample and reactants were significantly reduced (Lion et al. 2004; Shang et al. 2012; Freemantle 1999; Jacobson et al. 1998). More recently, with the purpose of integrating all routine assays of molecular biology in a single device (Haeberle and Zengerle 2007; Thorsen et al. 2002), new materials such as polydimethylsiloxane (PDMS) began to be used (Friend and Yeo 2010). Different designs have been reported in the literature (Keynton et al. 2004; Tran et al. 2010; Wu et al. 2008), and several devices are commercially available at present.

The vast majority of these devices consist of a network of rectilinear channels connected to reservoirs, which also serve as the point of application of electric potentials. Consequently the space available for electrophoresis is limited by the extension of the channels, between 1 and 5 cm, which in turn requires the application of voltages on the order of 1 kV to achieve analysis times between 10 and 120 s. The resulting field strengths attempt against the integrity of both the device itself and the fluids, and favor the occurrence of pernicious effects, such as Joule heating and bubble formation.

In order to overcome these difficulties, we present a device, baptized as “*Biotron*”, that includes a closed-loop microchannel of circular shape and a set of electrodes

---

**Electronic supplementary material** The online version of this article (doi:10.1007/s00542-012-1678-7) contains supplementary material, which is available to authorized users.

---

B. Lerner (✉) · A. F. Ordoñez Arias · C. Lasorsa  
Grupo MEMS, Comisión Nacional de Energía Atómica,  
Buenos Aires, Argentina  
e-mail: blerner@cnea.gov.ar

B. Lerner · M. S. Perez  
Grupo de Ingeniería Bioquímica, Universidad de Buenos Aires,  
Buenos Aires, Argentina

P. A. Kler · C. L. A. Berli  
INTEC (UNL-CONICET), Güemes 3450,  
3000 Santa Fe, Argentina

M. S. Perez · C. Lasorsa  
Laboratorio de Procesamiento Por Plasma, Universidad  
Tecnológica Nacional, Buenos Aires, Argentina

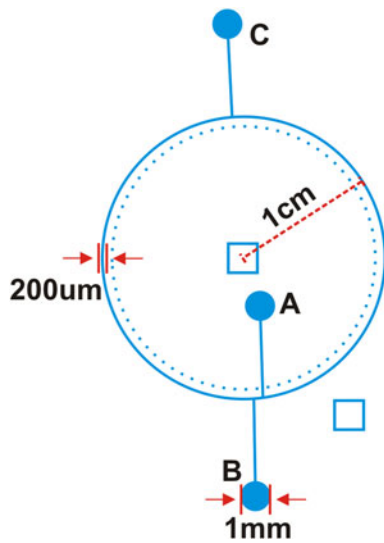


**Fig. 1** Design of the fluidic component of the *Biotron*. All channels have rectangular cross-section, 200  $\mu\text{m}$  in width and 25  $\mu\text{m}$  in depth

equally spaced along the channel. Microchannels were fabricated in PDMS and then bonded to a silicon wafer containing the previously deposited electrodes. The electrode spacing allows the application of DC voltages as low as 1 V. A suitable DC source, specifically built for the chip, is used to control the electric potentials and the application times, so that the circular microchannel can be virtually considered as an infinitely long separation channel. Of course, the working principle is the migration of macromolecules in a background fluid by means of electrokinetic forces. Therefore, to better understand and control electric forces in the system, our investigation includes 3D numerical calculations of the electric field in the microchannel. The electrophoretic transport of DNA samples was studied under different voltage configurations, and fluorescence microscopy was used for visualization. Experiments reported here demonstrate the functionality of the *Biotron*, and simultaneously show interesting features of electrokinetic transport of DNA.

## 2 Materials and methods

### 2.1 Device design

The system basically involves two components that respond to the operating principle of the *Biotron*: the fluidic layer containing the microchannels (Fig. 1), and the substrate with embedded electrodes (Fig. 2). The final device is obtained by joining the two constituent parts as shown in Fig. 3. The electrodes are thus located at the level of the bottom wall of the circular channel.

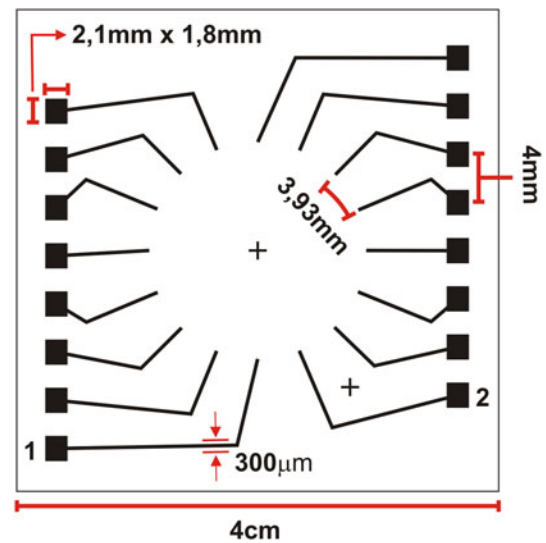


**Fig. 2** Design of the electrodes for the circular microchannel

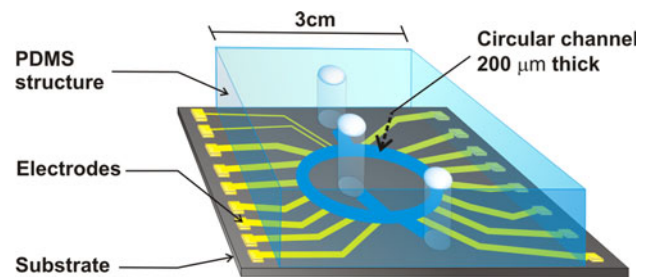


**Fig. 3** 3D scheme of the fluidic and electric layers arranged together

Reservoirs A and B (Fig. 1) are designed for the initial injection of DNA. The intersection of straight channels to the circular channel constitutes the injection zone, with a double-L configuration, which can dispense an approximate volume of 3 nL. The injection zone is filled with the sample by applying a potential difference between reservoirs A and B. Then the sample contained in the injection zone is moved through the circular channel by applying a voltage in the adjacent electrodes 1 and 2 (Fig. 2). The subsequent application of electric voltages between neighbor electrodes mobilizes the initial DNA element along the circular channel. The reservoir C (Fig. 1) is necessary to allow the complete filling of the channel with the polymeric matrix and the subsequent extraction of the samples.

### 2.2 Fabrication

Several microfabrication processes have been implemented. For the fluidic component, the fabrication scheme of Fig. 4 was followed. A mold of the design in high relief was made by photolithography in a silicon (100) wafer 700  $\mu\text{m}$  thick (Virginia Semiconductor, Inc.), by using the

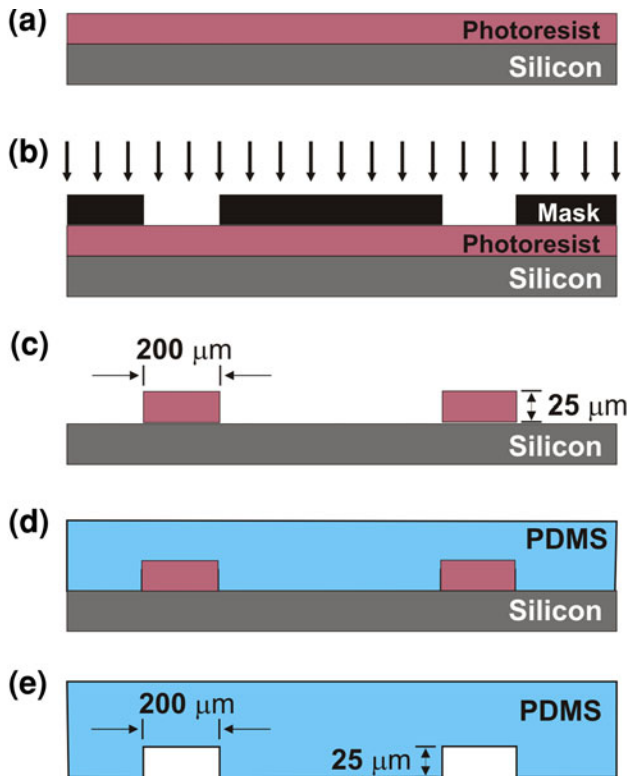


**Fig. 4** Manufacture of the fluidic device **a** deposition of resin on Si, **b** alignment of the mask and UV exposure, **c** result post revealed, **d** deposition of PDMS on the mask, **e** result in PDMS post cured

negative resin SU-8 (MicroChem). PDMS was mixed with curing agent in a 15:1 ratio. The mixture was placed under vacuum to remove air bubbles. After this, the mixture was poured into the master; placed under vacuum once again, and cured in an oven at 70 °C during 70 min. Finally the sample was peeled off. Microchannels ( $200 \pm 5$  μm thick and  $(25 \pm 0.5)$  μm in height) were obtained, as verified by scanning electron microscopy and profilometry (Lerner et al. 2012).

For the manufacture of the electrodes, a silicon (100) wafer 700 μm thick (Virginia Semiconductor, Inc.) covered with 200 nm thick  $\text{Si}_3\text{N}_4$  was used as the substrate. The negative of the electrode pattern was transferred implementing the same photolithographic technique of Fig. 4. A 30 nm Ti layer followed by a 120 nm Au layer were deposited by sputtering (AJA Sputtering System) (Iles and Pamme 2008). The Ti layer was intended to optimize adhesion of Au on the substrate. After lift-off process, the sacrificial layer formed by the resin and the metal was removed, leaving Au electrodes on the silicon wafer.

Once the processes were finished (PDMS microchannels and electrodes on silicon), both parts were joined by exposure to oxygen plasma in PECVD reactor (home-made equipment). Exposure to plasma was performed for 60 s, after which the PDMS and Si were contacted and

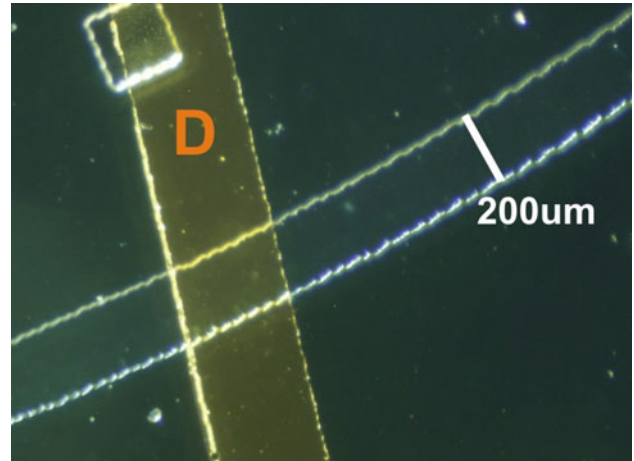


**Fig. 5** Optical microscopy image exhibiting one Au electrode (*D*) deposited by sputtering on Si, and a section of the PDMS circular microchannel passing over the electrode

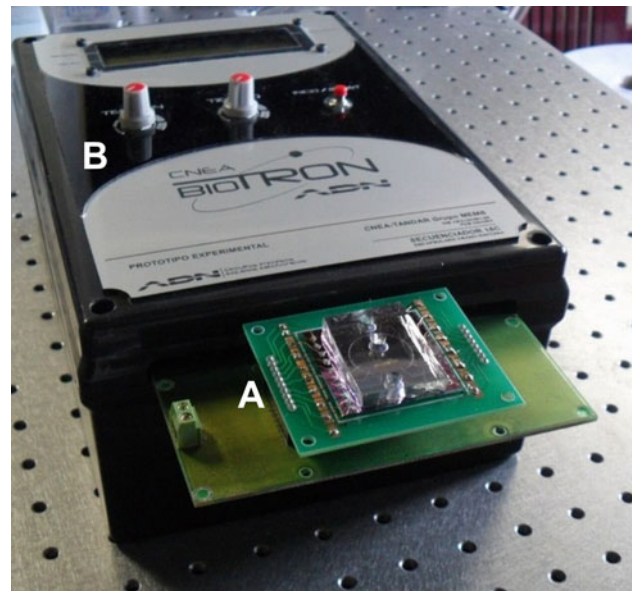


**Fig. 6** **a** Biotron coupled to the encapsulated and **b** variable voltage source

irreversibly joined. Figure 5 shows a section of the circular PDMS microchannel, with a transverse gold electrode integrated the bottom wall of the channel.

As a final step, the contact PADS on silicon were bonded to an external packaging that allows the connection of the chip to a DC voltage source specifically designed and build for the *Biotron* (Fig. 6). The source provides different output voltages, and can be programmed to sequentially control the magnitude of the electric potential and the application time on each electrode.

As a validation test, the electrophoretic migration of a DNA samples in the circular microchannel was compared to that in conventional linear microchannels. Therefore

parallel experiments were performed. For this purpose, linear microchannels were made following the technique of molding PDMS (Fig. 4), and a glass microscope slide (Biotraza) was used as substrate. The PDMS and the glass were joined by exposure to oxygen plasma. The linear channel was 200  $\mu\text{m}$  wide, 25  $\mu\text{m}$  high, and 4 cm long, with reservoirs at its ends.

### 2.3 Mathematical model and software

The electrokinetic velocity developed by a particle under the action of an electric field of strength  $E$  is due to the combination of electroosmosis and electrophoresis, and can be written  $v_{\text{EK}} = \mu_{\text{EK}}E$ , where  $\mu_{\text{EK}}$  is the electrokinetic mobility. In addition, since electrodes are arranged on the surface of the canal, strong electric field gradients may take place in near the electrodes, giving rise to dielectrophoretic forces. The dielectrophoretic velocity developed by a particle can be written  $v_{\text{DEP}} = \mu_{\text{DEP}}\nabla E^2$ , where  $\mu_{\text{DEP}}$  is the dielectrophoretic mobility (Li 2004). Therefore, given the paramount importance of attaining an appropriate control of the electric forces in the microchannel, here we numerically calculate the electric field  $E(x,y,z) = -\nabla\phi(x,y,z)$  in the 3D fluid domain of the circular microchannel containing a series of integrated electrodes (Fig. 7). In the Cartesian coordinate system,  $x$ - $y$  define the plane that contains the circular microchannel, while the  $z$  coordinate measures the vertical distances. The total electric potential  $\phi(x,y,z)$  is governed by Poisson equation,  $\nabla^2\phi(x,y,z) = -\rho/\epsilon$ ,

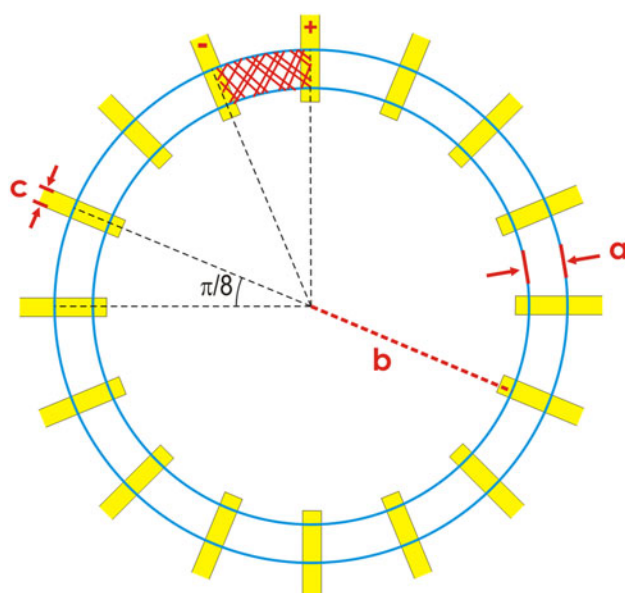


**Fig. 7** Mathematical domain for the simulations of the electric field. Channel thickness (a), loop radius (b), and electrodes thickness (c), are specified in the text for each calculation

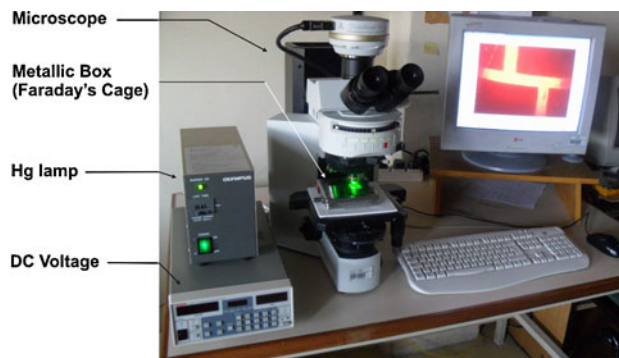


**Fig. 8** Experimental setup for DNA electrophoresis experiments on the manufactured devices

where  $\rho$  is the electric charge density and  $\epsilon$  is the permittivity of the medium (Li 2004).

The first contribution to the electric field is due to the potential difference applied at the electrodes. There is an additional potential in the fluid domain that comes from the presence of electrostatic charges at solid–liquid interfaces, which induce the electrical double layer of ions in solution. The thickness of this layer is on the order of 1–10 nm for the ionic concentrations normally used in practice, while cross-sectional channel dimensions are 200  $\mu\text{m}$ . Therefore, the surface potential is disregarded for the purposes of this work. In addition, assuming that electrolyte concentrations are uniform throughout the fluid ( $\rho = 0$ ), the right-hand side of Poisson equation vanishes, and the electric field is governed by Laplace equation,  $\nabla^2\phi(x,y,z) = 0$ . Under the circumstances, the field lines are expected to depend on the geometrical features of the microchannel and electrodes only. Microchannel walls were supposed perfectly isolating, as a first approximation.

Numerical calculations were carried out by using PETSc-FEM, a parallel multiphysics code primarily targeted to 2D and 3D finite elements computations on general unstructured grids. In particular, electric field computations were carried out with the charge conservation module, and transport equation are solved using the electrophoresis module. Visualization and post-processing are carried out in Paraview 3.6. Further details are given in Kler et al. (2011).

### 2.4 Electrophoresis and detection

For experimental runs, 2 % agarose (Sigma-Aldrich) in 0.5X Tris–Borate-EDTA (TBE) was used as the background matrix. The liquid agarose was placed in one of the seed reservoirs and all channels were filled by capillarity. For electrophoretic runs, a single-stranded DNA fragment of 20 bases (AGC TAG TCG CTA AAG TGG AC) called *swm13* (Sigma-Aldrich) was employed. The fluorophore TAMRA (Sigma-Aldrich) covalently joined to the 5'

terminal sequence of the primer *swm13* was used for detection.

At the beginning of each experiment, 3  $\mu\text{L}$  of DNA in a concentration of 0.5  $\mu\text{g}/\mu\text{L}$  were deposited on the seed reservoir. Visualization was performed by using a fluorescence microscope Olympus BX51K, which has an integrated camera that allows real-time detection and data storing in a PC for further analysis.

The electrical voltage was applied with the DC voltage source (Fig. 6) in the case of the *Biotron*, and in the linear

channels with a high voltage source Keithley 248. In the linear channel device, Pt electrodes were used to apply tension in the reservoirs, which are positioned inside a metal box (Faraday cage) to avoid accidental discharges into the microscope. Figure 8 shows the experimental set up performed.

### 3 Results

This section illustrates the simulations done to study the behavior of the electric field inside the circular channel with electrodes included within. Also it shows some particular effects of DNA migration in the circular microchannel due to the characteristics of the electric field discussed in the simulations. For this purpose, a series of electrophoresis experiments were performed for different configurations of the applied electric potential.

#### 3.1 Electric field simulations

##### 3.1.1 2D analysis

Firstly we explored the 2D electric field of the whole microchannel in the  $x,y$  plane. A potential difference of 20 V is applied between two arbitrary electrodes, as indicated by the arrows in Fig. 9. Geometrical dimensions used in these calculations are the following: channel width, 600  $\mu\text{m}$ ; radius of the microchannel loop, 25 mm; electrodes width, 100  $\mu\text{m}$ . It is worth noting that, since the loop is closed, the potential decreases from 20 to 0 V along the two possible ways between the active electrodes.

Figure 10 shows the resulting electric field, which is quite homogeneous along the channel, except in the close vicinity of the connected electrodes. As the field strength

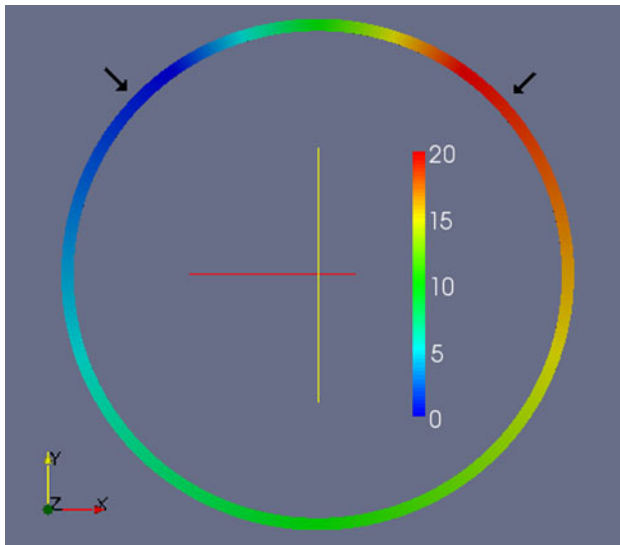


**Fig. 9** Electrical potential in the circular microchannel when a potential difference of 20 V is applied between two electrodes, the position of which is indicated by the arrows

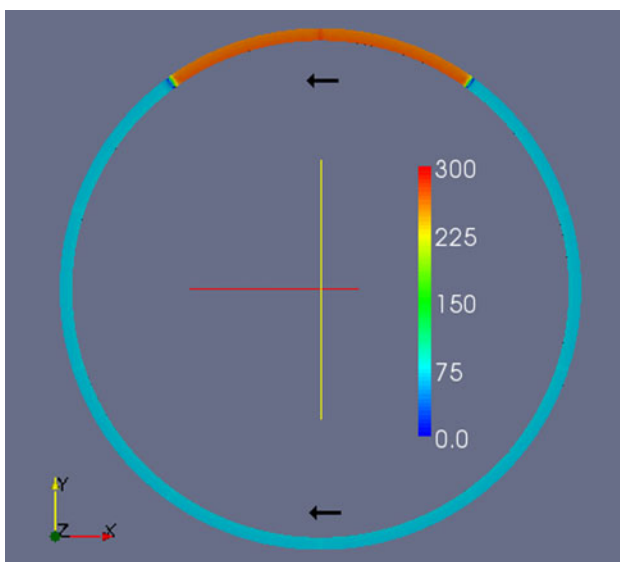


**Fig. 10** Electrical field in the circular microchannel corresponding to the voltage applied in Fig. 9. Numerical values of  $E$  are in V/m. Arrows indicate the direction of  $E$

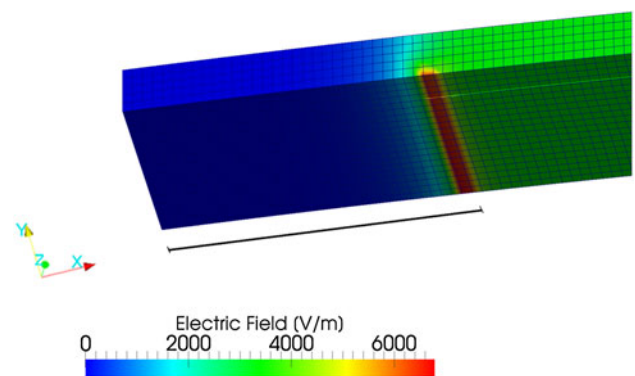


**Fig. 11** Electrical field in the region of an active electrode, when a potential difference of 12 V is applied. The calculation domain comprises half width electrode (indicated by the black bar) and a portion of the channel (right side). The microchannel is seen from the bottom wall

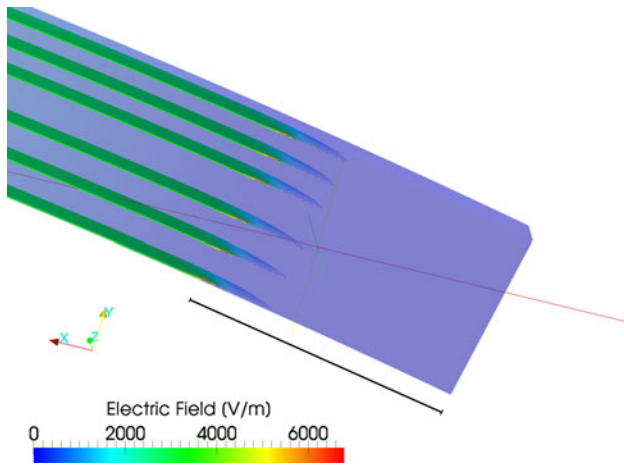


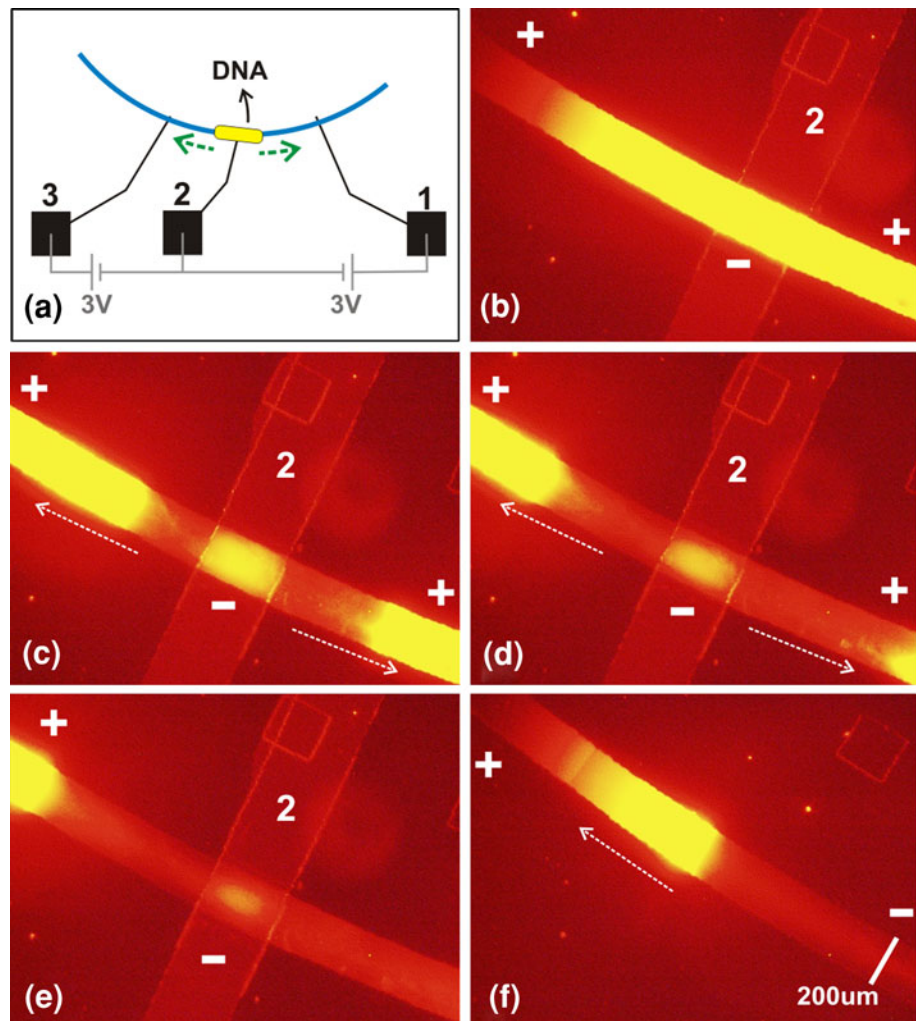
**Fig. 12** Electrical field lines over the active electrode, when a potential difference of 12 V is applied. The computation domain is that described in Fig. 10, now seen from the top wall, with the electrode on the right, as indicated by the *black bar*

depends on separation between the electrodes,  $E$  is higher in the upper zone of the loop (orange region in Fig. 10) than in the lower one (light blue region). The direction of  $E$  is from the highest potential to the lower one, i.e., from right to left in both the upper (orange) and lower (light blue) zones of the loop.

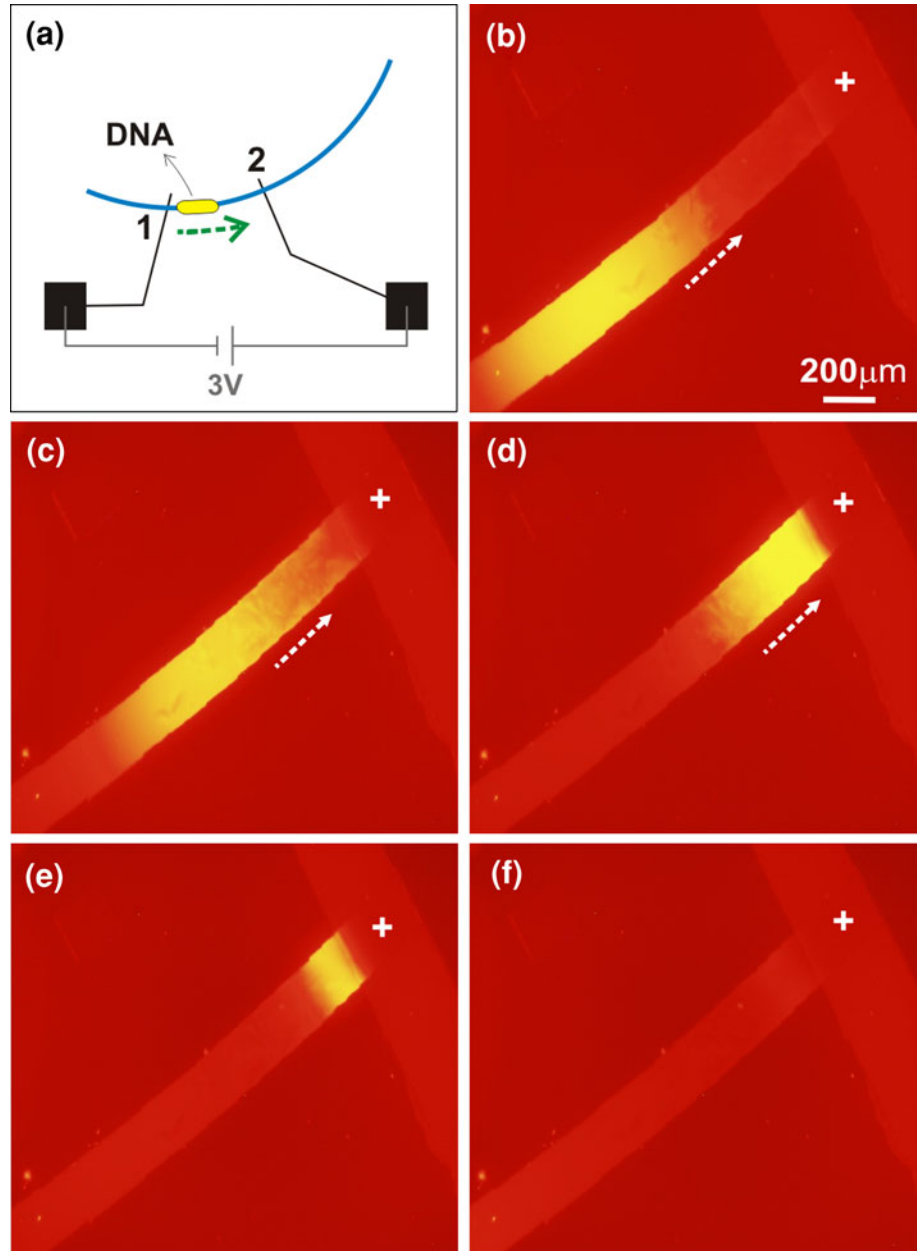
### 3.1.2 3D analysis

In what follows we present 3D simulations of the electric field in the region of the electrodes, which is relevant to interpret DNA migration, as it is discussed below in DNA Electrophoresis section. For the purposes we considered the computational domain indicated by the red mesh in Fig. 7, which correspond to the volume confined between two consecutive electrodes. Geometrical dimensions used are: channel width, 200  $\mu\text{m}$ ; radius of the microchannel loop, 10 mm; electrodes width, 300  $\mu\text{m}$ ; the separation

**Fig. 13 a** Scheme showing the initial position of DNA sample and the voltage configuration used, **b–f** fluorescence microscopy images corresponding to DNA migration at different times, with intervals of 2 s



**Fig. 14** **a** Scheme showing the initial position of DNA sample and the voltage configuration used, **b–f** fluorescence microscopy images corresponding to DNA migration at different times, with intervals of 2 s



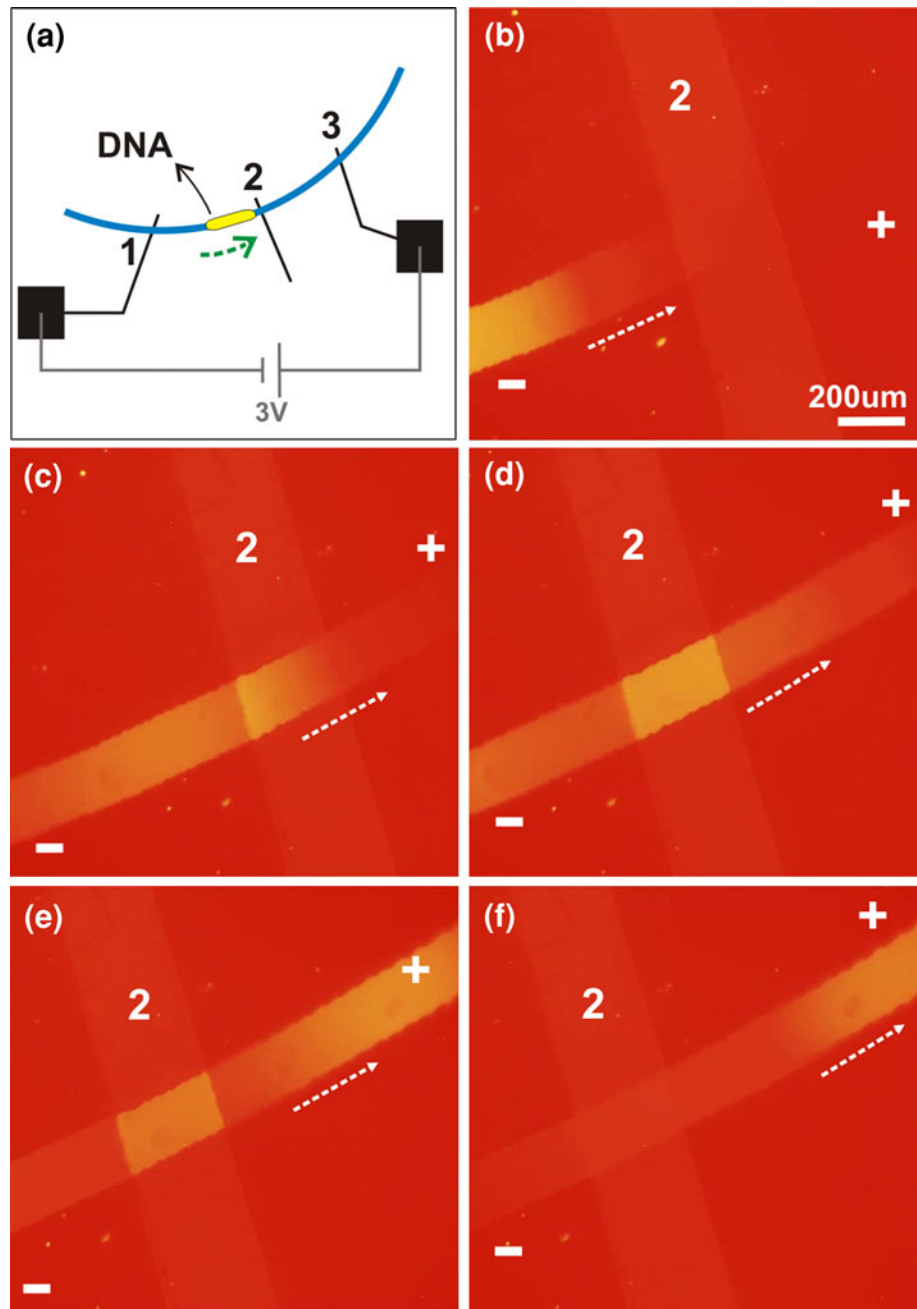
between electrodes is the arc corresponding to  $\pi/8$  radians of the circle (Fig. 7).

Figure 11 shows the electric field  $E$  in the 3D domain, when the applied potential difference is 12 V (the black bar indicates the position of half electrode). Channel walls were assumed to be perfectly isolating, thus field lines follow uniformly the axial direction of the channel, and intercept the walls only at electrode surfaces. More precisely, lines enter/exit the electrode at the border, where the field becomes relatively high, as denoted by the red (hot) zone in Fig. 11. Consistently, the electric field completely

vanishes in the middle zone of the electrodes, which is the blue (cold) zone in Fig. 11.

Further insights on the shape of field lines around electrode surfaces are obtained from Fig. 12, which presents an upper view of the channel in the close region of the electrode. Again one observes that a pronounced field gradient takes place at the electrode border. Apart from electrophoretic forces ( $\propto E$ ), these field lines are capable to generate strong dielectrophoretic forces ( $\propto \nabla E^2$ ) that can trap DNA molecules on the electrode surface, notably at the electrode border with high field strength. These

**Fig. 15** **a** Scheme showing the initial position of DNA sample and the voltage configuration used, **b–f** fluorescence microscopy images corresponding to DNA migration at different times, with intervals of 2 s



characteristics of  $E$  have relevant effects on the migration of DNA molecules, as discussed below in DNA electrophoresis section.

### 3.2 DNA electrophoresis

Electrophoresis experiments were conducted in the *Biotron*, where different configurations of applied electric potential between electrodes were studied. Then measured of DNA mobility in the *Biotron* and linear channels were done to compare the behavior of DNA in both geometries.

#### 3.2.1 DNA migration from a negative electrode

A volume element of DNA was situated on electrode 2, and then a potential difference of 3 V was applied between electrodes 1 and 2, as well as between electrodes 2 and 3, as shown schematically in Fig. 13a. Figure 13b–f shows the migration of DNA at different times. The time elapsed between each image is 2 s. Given the negative charge of DNA, the electrophoretic migration takes place from the negative electrode (2) towards the positive electrodes (1 and 3). The electric field strength between the electrodes

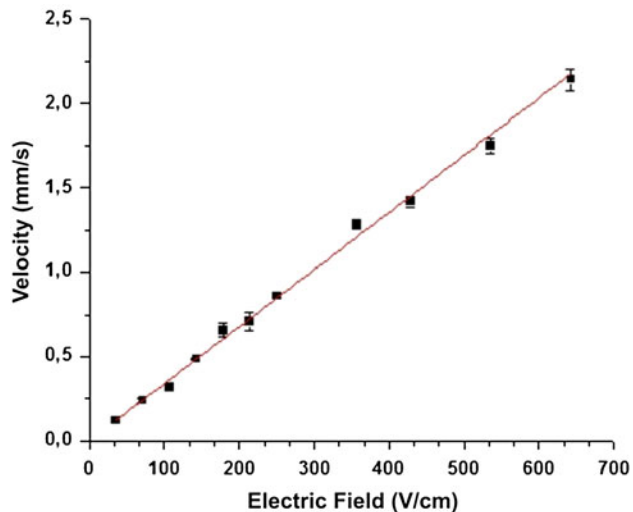


**Fig. 16** Velocity of the *swm13* primer to different electrical fields applied in linear channels

1 and 2 is equal to that between electrodes 2 and 3, but the field lines go in opposite directions. Therefore the initial DNA element is divided into two fractions (Fig. 13c), which move away from the negative electrode at the same speed (see video S1 in Supplementary information).

Figure 13c–e shows that the DNA located at the sides of the electrode 2 migrates immediately after the potential is applied, while the DNA located over the electrode 2 took a longer time to migrate. This experimental result agrees with the simulations of the electric field presented above (Figs. 11, 12): the  $E$  field is intense at the edges of the electrode, and decreases gradually to vanish completely in the middle of it.

### 3.2.2 DNA adsorption on positive electrodes

A volume element of DNA was situated between electrodes 1 and 2, and then a potential difference of 3 V was applied between them, as shown in Fig. 14a. Figure 14b, c show conventional DNA migration toward the positive electrode. Figure 14d–f show DNA behavior when reaching the electrode 2 (see video S2 in Supplementary information).

In this experiment DNA molecules result irreversibly adsorbed at the edge of the positive electrode. In this region the electric field reaches very high values, as predicted in Figs. 11 and 12. In addition, the sharp field gradients can generate strong dielectrophoretic forces that contribute to the absorption of DNA on the electrode. This effect is discussed here to make emphasis on the electric field. Of course, DNA adsorption and loss of sample are not desired effects in conventional electrophoretic analysis. In our device, the phenomenon can be avoided with an appropriate configuration of potentials, as is showed in the next section.

### 3.2.3 DNA migration over a neutral electrode

A volume element of DNA was situated between electrodes 1 and 2, and then a potential difference of 3 V was applied between electrodes 1 and 3, as shown in Fig. 15a. Figure 15b–f show the migration of DNA at different times (see video S3 in Supplementary information).

The first aspect to be noted is that DNA does not adsorb on the neutral electrode (2). Nevertheless, it is interesting to observe a sort of pre-concentration of the DNA during the transit over electrode 2 (Fig. 15c–e). This phenomenon is due to the fact that the electrical conductivity of the electrode is higher than that of the rest of the channel walls, therefore some field lines may intercept the electrode surface, even when it is floating (the electrode surface is not perfectly isolating indeed). These field lines constitute a dielectrophoretic trap for negatively charged particles, and different potential applications are envisaged. On the other hand, to avoid this effect in electrophoretic runs, the passivation of the substrate by evaporation of a silicon nitride layer over the electrodes is planned for future experiments.

### 3.2.4 Comparison of the migration between linear and circular channel

Experiments were conducted in which the DNA speed in function of the applied electric field was measured and the mobility of the sample was determined. The mobility values for *swm13* DNA were compared in experiments with agarose 2 % performed on devices with circular and linear channels.

The DNA mobility for *swm13* in linear channels was  $(3.3 \pm 0.1) \times 10^{-4} \text{ cm}^2/\text{V}\cdot\text{s}$  (Fig. 16) and for circular channels was  $(3.2 \pm 0.1) \times 10^{-4} \text{ cm}^2/\text{V}\cdot\text{s}$ .

There was, thus, a correspondence between the results obtained that show that the direct contact between the electrodes and the agarose in the circular channel, and the closed geometry of this, do not affect the mobility of the samples.

Although the *Biotron* showed to be able to migrate the DNA similarly to linear devices commonly used in electrophoresis of DNA, it is still necessary to conduct further studies to avoid processes such as diffusion. Applying different configurations of potential between electrodes in order to concentrate the DNA is thought to skip the diffusion phenomenon thus allowing run with the DNA greater distances.

## 4 Conclusions

An alternative approach to implement electrophoresis on chips is presented, which opens new possibilities in the

field of DNA analysis. In fact, the circular geometry of the closed-loop microchannel, as well as the disposition of embedded electrodes, offers several advantages: using low potentials to obtaining high electric fields, the possibility of using a relatively long separation channel (virtually infinite), and further potential applications such as dielectrophoretic manipulation.

A crucial aspect of this work is that, in parallel to the tasks of design, modeling, construction, and testing, computer simulations were performed to investigate the electric field into the microchannel. The realized simulations allowed understand the behavior of the field within the channels and explain the observed phenomenon of DNA absorption in the edge of the positive electrode.

**Acknowledgments** CLAB thanks the financial support from CONICET (PIP 0317) and Universidad Nacional del Litoral (CAI + D65/328), Argentina. We would like to thank M.J. Dieguez, F. Sacco and E.M. Salmoral for technical advice and discussion.

## References

- Andrews AT, Andrews A (1986) *Electrophoresis: theory, techniques, and biochemical and clinical applications*, vol 148. Clarendon Press, Oxford
- Freemantle M (1999) Downsizing chemistry: chemical analysis and synthesis on microchips promise a variety of potential benefits. *Chem Eng News* 77(8):27–36
- Friend J, Yeo L (2010) Fabrication of microfluidic devices using polydimethylsiloxane. *Biomicrofluidics* 4:026502
- Haeberle S, Zengerle R (2007) Microfluidic platforms for lab-on-a-chip applications. *Lab Chip* 7(9):1094–1110
- Hames B (1998) *Gel electrophoresis of proteins: a practical approach*, vol 197. Oxford University Press, USA
- Harrison DJ, Fluri K, Seiler K, Fan Z, Effenhauser CS, Manz A (1993) Micromachining a miniaturized capillary electrophoresis-based chemical analysis system on a chip. *Science* 261(5123):895–897
- Iles A, Pamme N (2008) Sputtering for Film Deposition. In: *Encyclopedia of microfluidics and nanofluidics*. Springer, New York p 1882
- Jacobson SC, Culbertson CT, Daler JE, Ramsey JM (1998) Microchip structures for submillisecond electrophoresis. *Anal Chem* 70(16):3476–3480
- Keynton R, Roussel T, Crain M, Jackson D, Franco D, Naber J, Walsh K, Baldwin R (2004) Design and development of microfabricated capillary electrophoresis devices with electrochemical detection. *Anal Chim Acta* 507(1):95–105
- Kler PA, Berli CLA, Guarnieri FA (2011) Modeling and high performance simulation of electrophoretic techniques in microfluidic chips. *Microfluid Nanofluid* 10(1):187–198
- Lerner B, Perez MS, Kler P, Berli CLA, Ordoñez Arias A, Sacco F, Toro C, Rinaldi C (2012) Laser fabrication of micropores and their integration to microfluidic platforms for DNA electrophoresis. *Microsyst Technol* 18(4):429–435
- Li D (2004) *Electrokinetics in microfluidics*. Elsevier Academic Press, London
- Lion N, Reymond F, Girault HH, Rossier JS (2004) Why the move to microfluidics for protein analysis? *Curr Opin Biotechnol* 15(1):31–37
- Shang F, Guihen E, Glennon JD (2012) Recent advances in miniaturisation—the role of microchip electrophoresis in clinical analysis. *Electrophoresis* 33(1):105–116
- Thorsen T, Maerkl SJ, Quake SR (2002) Microfluidic large-scale integration. *Science* 298(5593):580–584
- Tran NT, Ayed I, Pallandre A, Taverna M (2010) Recent innovations in protein separation on microchips by electrophoretic methods: an update. *Electrophoresis* 31(1):147–173
- Wu D, Qin J, Lin B (2008) Electrophoretic separations on microfluidic chips. *J Chromatogr A* 1184(1):542–559